

Local Convolutions Cause an Implicit Bias towards High Frequency Adversarial Examples

Josue Ortega Caro^{1,2,+}, Yilong Ju³, Ryan Pyle¹, Sourav Dey⁴, Wieland Brendel⁵, Fabio Anselmi¹, and Ankit B Patel^{1,6}

¹Department of Neuroscience, Baylor College of Medicine, Houston, TX, 77030

²Quantitative and Computational Bioscience Program, Baylor College of Medicine, Houston, TX, 77030

³Department of Computer Science, Rice University, Houston, TX, 77005

⁴Manifold AI

⁵University of Tübingen, Germany,

⁶Department of Electrical and Computer Engineering, Rice University, Houston, TX, 77005

⁺Correspondence to: caro@bcm.edu

Abstract

Despite great efforts, neural networks are still prone to adversarial attacks. Recent work has shown that adversarial perturbations typically contain high-frequency features, but the root cause of this phenomenon remains unknown. Inspired by the theoretical work in *linear full-width convolutional models* [1], we hypothesize that the *nonlinear local* (i.e. *bounded-width*) *convolutional models* used in practice are *implicitly* biased to learn high frequency features, and that this is the root cause of high frequency adversarial examples. To test this hypothesis, we analyzed the impact of different choices of linear and *nonlinear* architectures on the implicit bias of the learned features and the adversarial perturbations, in both spatial and frequency domains. We find that the high-frequency adversarial perturbations are critically dependent on the convolution operation in two ways: (i) the translation invariance of the convolution induces an *implicit* bias towards sparsity in the frequency domain; and (ii) the spatially-limited nature of *local* convolutions induces an implicit bias towards *high* frequency features. The explanation for the latter involves the Fourier Uncertainty Principle: a spatially-limited (local in the space domain) filter cannot also be frequency-limited (local in the frequency domain). Furthermore, using larger convolution kernel sizes or avoiding convolutions altogether (e.g. by using Visual Transformers architecture) significantly reduces this high frequency bias, but not the overall susceptibility to attacks. Looking forward, our work strongly suggests that understanding and controlling the implicit bias of architectures will be essential for achieving adversarial robustness.

1 Introduction

Despite the enormous progress in training neural networks to solve hard tasks, they remain surprisingly and stubbornly sensitive to imperceptibly small worst-case perturbations known as *adversarial examples*. This lack of robustness has sparked many theories [2–9], but a unified theoretical explanation of the nature of adversarial examples is still lacking.

Recent work [10] has shown that commonly found adversarial examples for state-of-the-art convolutional neural networks are mainly composed of high frequency information. In addition, they found that adversarial perturbations of naturally trained models tend to be higher frequency as compared to

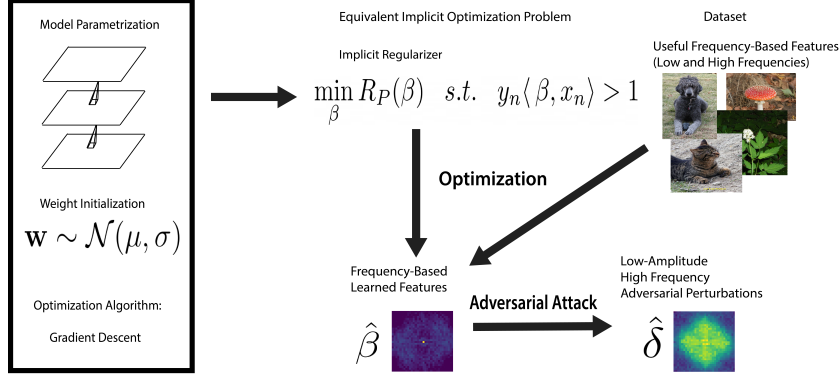


Figure 1: The Implicit Fourier Regularization (IFR) Hypothesis. Model parametrization and weight initialization induces an implicit optimization bias. This will lead to different learned features β and therefore, different adversarial perturbations δ . In particular, implicit regularization in the frequency domain, directly caused by the translation invariance of the convolution operation, is necessary for the evolution of frequency-based features. Furthermore, the spatially-limited nature of common local convolutional operations encourages the learned features β to possess energy in *higher* frequencies.

those of adversarially trained models. This line of work suggests that a frequency-based understanding of model robustness might be an important step towards building robust, interpretable models. A natural question arises: Why *frequencies*, as opposed to some other basis?

Here we propose an answer to this question that relies on the concept of *implicit bias*. The idea behind implicit bias is that the loss landscape of an overparameterized network has infinitely many global minima, and which global minimum one converges to after training depends on many factors, including the choice of model architecture/parametrization [1, 11], initialization scheme [12] and optimization algorithm [13–15]. The implicit bias of state-of-the-art models has been shown to play a critical role in the generalization of deep neural networks [16, 17]. Recent theoretical work [1] on *L*-layer *deep linear networks* has revealed that (i) fully connected layers induce a depth-independent ridge (ℓ_2) regularizer in the spatial domain whereas, surprisingly, *full-width convolutional layers* induce a depth-dependent *sparsity* ($\ell_{2/L}$) regularizer in the *frequency* domain. Linear full-width convolutional models are different from the high-performance convolutional neural networks (CNNs) used in practice. Nonetheless, we hypothesised that similar mechanisms might play a role for *deep nonlinear models with local convolutions*, meaning that the high frequency nature of commonly found adversarial perturbations is due to the implicit bias induced by the specific architectural choice. More formally, we propose the Implicit Fourier Regularization (IFR) hypothesis (see Figure 1):

Implicit regularization in frequency domain, directly caused by the translation invariance and spatially limited nature of bounded-width convolutions, yields a strong bias towards high frequency features and adversarial perturbations.

The IFR hypothesis can be decomposed into three parts, and we will provide evidence for each later on in the paper. First, convolutions, due to their translation invariant nature, induce an implicit bias promoting sparsity in the Fourier domain for *nonlinear CNNs* with full-width convolutions (thereby extending theoretical results on *linear models* [1]). Second, restricting to bounded-width (spatially limited/localized) convolutions changes the implicit bias, encouraging the linear features to possess energy in *high* frequencies; this arises because a space-limited filter cannot also be band-limited, a mathematical consequence of the Fourier Uncertainty Principle. Third, the high frequency features learned by the model in turn induce high frequency adversarial perturbations.

Our specific contributions are as follows:

- Based on extensive, systematic experiments, we show that different model parametrizations have very different spectra in their learned features and adversarial perturbations (see Figure 2).

- We derive new theoretical results for deep linear models with bounded-width convolutions, showing that the spatially-limited nature of local convolutions induces an implicit bias towards high-frequency features. This is confirmation of the IFR hypothesis for linear models.
- We confirm a similar bias empirically for deep nonlinear models with bounded-width convolutions, thereby showing that the spatially-limited nature of local convolutions is critical to explaining high frequency features and adversarial perturbations (see Figure 2). This is confirmation of the IFR hypothesis for nonlinear models.
- Through a novel class of steganography-inspired experiments, we confirm that the $\ell_{\frac{2}{L}}$ Fourier regularizer, proposed by [1] for linear models, is also present in *nonlinear* models with full-width convolutions (see Table 2).
- By exploring the learning dynamics, we show that adversarial examples evolve from low to high frequency throughout optimization (see Figure 4, 5).
- Finally we show that Visual Transformers [18], a state-of-the-art model architecture that avoids convolutions, has adversarial perturbations with less energy in the high frequencies (see Figure 6).

2 Related Work

Explanations of Adversarial Examples. Researchers have tried to understand the conditions that are necessary for adversarial perturbations to arise. Some work has focused on statistical properties of the data distribution [2–6], whereas other work has studied overfitting or underfitting [7–9]. See [19] for a comprehensive review. However, to our knowledge, no existing work has used learning dynamics or implicit regularization theory to understand both the evolution and the high frequency bias of adversarial features.

Fourier Analysis of Input Perturbations. Recent work on understanding how data augmentation techniques can improve robustness to adversarial and noise perturbations has adopted a Fourier perspective [19, 20]. For example, in [19] the authors find that adversarial training (and other forms of noise perturbations) produce models which are robust to high frequency noise.

Our work takes a different point of view: we explore how and why adversarial attacks on convolutional models (as compared to other model parametrizations) produce high frequency features and perturbations in the first place.

Relationship between Generalization and Adversarial Attacks. Some work has studied the relationship between performance and adversarial development. In [21] the authors establish that for certain loss functions, adversarial examples are inescapable and that input complexity could affect the robustness of the model. In addition, [19, 22–24] have found that, for classification problems, non-robust features *improve* the performance of the classifier, and that adversarial robustness is at odds with accuracy.

Theories of Learning Dynamics & Implicit Regularization. This line of theoretical work aims to understand the generalization properties of *overparameterized* neural networks [13, 1, 25, 14]. Early work revealed the surprising phenomenon of *implicit regularization*: When a loss surface possesses many *global* minima of equal value, which is common in overparametrized models, the specific global minima that a learning algorithm converges to can depend greatly on seemingly irrelevant details such as the choice of weight initialization method, learning algorithm, and model parametrization.

Recent studies have also shown that such implicit regularization/bias is responsible for much (if not most) of the generalization performance of state-of-the-art image classifiers [16, 17]. Our work builds on recent work [1] that proves that overparameterized deep linear models with and without convolutions induce dramatically different implicit biases, the former yielding a bias towards features that are sparse in the *Fourier* domain. Furthermore, we demonstrate experimentally that this is also the case for non-linear models.

3 Experimental Results

3.1 Impact of Model Parametrization on Adversarial Perturbations

Recent theoretical work [1] has shown that shallow linear convolutional neural networks with a single hidden layer (**full-width circular** convolutional linear layers followed by one **fully connected** linear layer) induce an implicit sparsity-promoting regularizer in the Fourier domain. Specifically, the regularizer is: $\mathcal{R}_{FWC}(\beta) = \|\hat{\beta}\|_2^{\frac{2}{L}}$ where $\hat{\beta} := \mathcal{F}\beta$ is the Discrete Fourier Transform (DFT) of the end-to-end linear transformation $\beta := W_2 W_1$ represented by the linear network and L is the number of layers. If this implicit bias affects the features learned by the model, could this also alter the nature of the adversarial perturbations?

3.1.1 Confirming Gunasekar et al. [1] results and relationship to adversarial perturbations

To test this, we selected the two model parametrizations considered in Gunasekar et al. [1], namely fully connected and full-width convolutional models. In addition, we used shallow (one hidden layer) and deep (three hidden layers) versions of these models, along with linear and nonlinear activation functions. These models were trained on CIFAR-10 dataset [26] (MIT) using PyTorch [27] (performance in Supp. Table 6).

Our goal here is to understand the relationship between the learned features β learned by these models and their corresponding adversarial perturbations δ . We computed β by extracting the plain saliency map (i.e. differentiating the logits with respect to the input image). Then, we used the Foolbox package [28] (MIT) to generate adversarial perturbations δ for every example in the test set for a fully trained model (PGD-Linf, PGD-L2, PGD-L1[29], BB-Linf and BB-L2 [30]). Finally, we compute the 2-D Discrete Fourier spectrum $\hat{\delta} := \mathcal{F}\delta$ of the perturbation δ . Details of the attacks are available in Table 11 in the Supplement.

In Figure 2, we can see the average Fourier spectrum of the adversarial perturbations ($\hat{\delta}$) for PGD-Linf and of the input-output weight visualization ($\hat{\beta}$). We observe that the full-width convolutional model (FWC) has a sparse spectrum of β compared to the fully connected model (FC), and when the model has more layers this difference increases (Deep FWC vs Deep FC). This is experimental confirmation of the theoretical result in [1] for linear models. Furthermore, to quantify the different sparsity levels of the two models, we measure the ℓ_1 and ℓ_2 norm of the Fourier spectrum of β for both the shallow and deep full-width and fully connected models (See Sup. Fig 10). We observe that the relationship between model parametrization and spectrum holds for the spectrum of the adversarial perturbations $\hat{\delta}$, where the full-width convolutional model has a sparse adversarial spectrum compared to the fully connected model. This was confirmed quantitatively by computing their Spearman correlation (see Table 1). These results also hold for the other attacks (see Supp. Figure 11, 12).

However, in contrast with theory, which predicts that $\delta \propto \beta$ for linear models, we instead find correlations < 1 [31, 8]. This is due to two reasons: (i) adversarial attacks are generated from randomly initialized perturbations that are uncorrelated with the input, thus reducing the correlation; and (ii) a successful adversarial attack requires only a minimal perturbation of the input such that the output category changes. As a consequence, the correlation between β and δ need not be maximal.

Next, we tested if the implicit regularizer has the same properties for nonlinear models. As we observe in Figure 2, the full-width convolutional model has a sparse spectrum of both β and δ compared to the fully connected model. This shows that the implicit regularizer due to the model holds for both linear and nonlinear models.

3.1.2 Expanding to Bounded-Width Convolutional Models

One limitation of this theory is that full-width convolutional layers are not often used in common state-of-the-art architectures. Bounded-width convolutional models are instead usually employed, which have smaller kernel sizes than the width of the input. Given this, we asked: what is the effect of the bounded-width convolutional model in $\hat{\beta}$ and $\hat{\delta}$?

To answer this question, we trained a bounded-width convolutional model and generated both $\hat{\beta}$ and $\hat{\delta}$ with the same procedure as the previous section. In Figure 2, we can see that the bounded-width

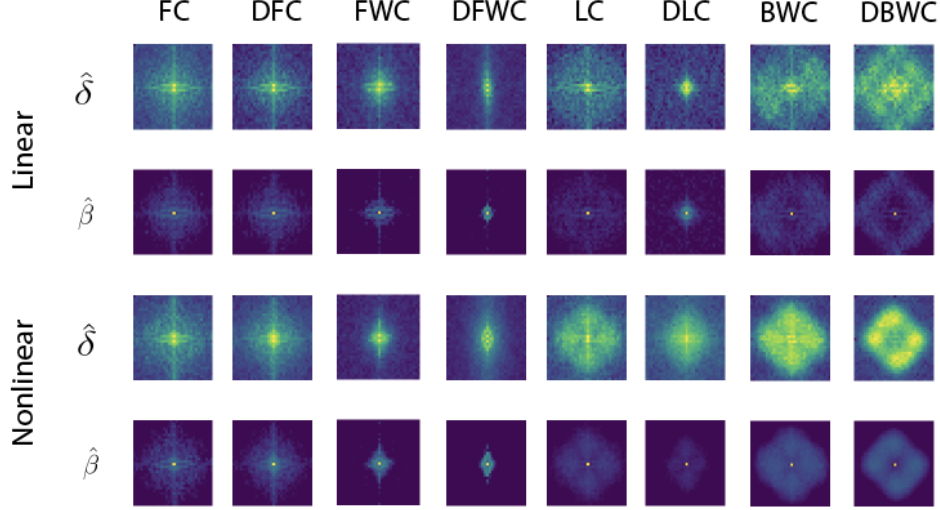


Figure 2: Average Frequency Spectrum of adversarial perturbation ($\hat{\delta}$) and input-output weights ($\hat{\beta}$) for Fully Connected (FC), Full-Width Convolutional (FWC), Locally Connected (LC) and Bounded-Width Convolutional (BWC) models for PGD-Linf Attack. We can observe the correlation between the input-output weights and the adversarial perturbations for each model. This results also hold for different attacks (See Sup. Figures 11, 12)

Table 1: Spearman Correlation between Fourier spectrum of Delta and Beta for different models.

Model	Spearman Correlation of $\hat{\beta}$ and $\hat{\delta}$	
	Linear Model	Nonlinear Model
Fully Connected	0.353	0.439
Deep Fully Connected	0.343	0.504
Full Width Convolutional	0.276	0.327
Deep Full Width Convolutional	0.272	0.452
Locally Connected Linear	0.240	0.275
Bounded Width Convolutional	0.266	0.371
Deep Bounded Width Convolutional	0.306	0.344

convolutional models (both linear and nonlinear) contain high frequency components in $\hat{\delta}$. This is further exacerbated by depth in the Deep Bounded-Width model (DBWC). Moreover, we observe that the β corresponding to the bounded-width convolutional model is as sparse or less sparse (more dense) compared to the full-width counterpart (see Supp. Figure 10).

Given that the theory [1] only specifies a bias towards ℓ_2 -sparsity in the frequency domain (support can consist of low or high frequencies), then why do we observe so much more energy in the higher frequencies of the bounded-width convolutional model but not the full-width convolutional model? Our experiments suggest that this is due to *the spatial locality constraint* imposed in the bounded-width convolutions. We propose a theoretical explanation via the Fourier Uncertainty Principle – a space-limited kernel *cannot* be band-limited in frequency domain – as the origin of frequency dispersion. The frequency dispersion is in tension with the sparsity promotion predicted by the implicit sparse Fourier regularizer, resulting in a compromise sparsity that is lower than that of the full-width convolutional model.

This reasoning can be made rigorous for a bounded-width linear convolutional model by a simple and straightforward extension of the results of [1], as follows.

Lemma 1. *Let the parametrization map be for a linear full-width convolutional networks be $\mathcal{P}_{FWC}(\mathbf{w}) = \left(((\mathbf{w}_L^\downarrow \star \mathbf{w}_{L-1}) \star \mathbf{w}_{L-2}) \dots \star \mathbf{w}_1 \right)^\downarrow$, $\mathbf{w} \in \mathbb{R}^D$, where \mathbf{w}^\downarrow denotes the flipped vector corresponding to \mathbf{w} , given by $\mathbf{w}^\downarrow[k] = \mathbf{w}[D - k - 1]$ for $k \in [D]$. Furthermore let*

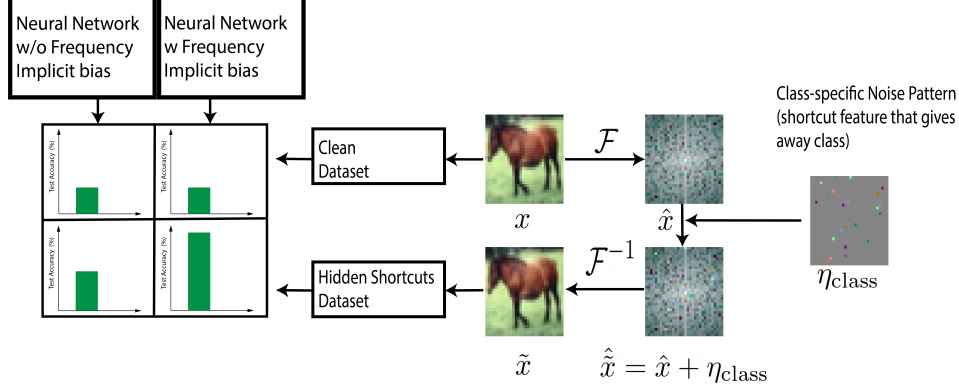


Figure 3: Steganography experiment. Class specific information η_{class} introduced into Fourier Spectrum of training set image ($\hat{\tilde{x}} = \hat{x} + \eta_{class} : \eta_{class} = M_{class} \odot (\epsilon * N_{class})$, $N_{class} \sim \mathcal{N}(0, 1)$, $M_{class} \sim \text{Bernoulli}(\rho)$). Models with sparse frequency regularizer (Full-Width and Bounded-Width Convolutional models) should take more advantage of hidden shortcut features in the dataset, therefore leading to higher test accuracy.

$\mathcal{C}_{l,d} := \{\mathbf{w}_l \in \mathbb{R}^{D_l} : \mathbf{w}_l[i] = 0 \forall i \notin [d]\}$ be the convex constraint set of bounded width (spatially limited) filters, where $d < D$ defines the support of \mathbf{w}_l . Then for a depth L bounded width d (a.k.a. locally connected) linear convolutional network with parameters $\mathbf{w} = [\mathbf{w}_l \in \mathbb{R}^{D_l}]_{l=1}^L$ and parameterization map $\mathcal{P}_{BWC}(\mathbf{w})$, the implicit regularizer is

$$\mathcal{R}_{\mathcal{P}_{BWC}}(\beta) = \min_{\mathbf{w} : \mathcal{P}_{BWC}(\mathbf{w}) = \beta} \|\mathbf{w}\|_2^2 \text{ s.t. } \mathbf{w}_l \in \mathcal{C}_{l,d} \forall l \in [L].$$

Proof. Recall that for linear predictors parameterized as $\beta = \mathcal{P}(\mathbf{w})$ that the implicit regularizer is $\mathcal{R}_{\mathcal{P}}(\beta) = \min_{\mathbf{w} : \mathcal{P}(\mathbf{w}) = \beta} \|\mathbf{w}\|_2^2$ (see Theorem 4 and Eqn. (15) in [1]). Substituting in the bounded-width convolutional parametrization $\mathcal{P} = \mathcal{P}_{BWC}$ and noting that the constraint set $\{\mathbf{w} : \mathcal{P}_{BWC}(\mathbf{w}) = \beta\} = \{\mathbf{w} : \mathcal{P}_{FWC}(\mathbf{w}) = \beta\} \cap \{\mathbf{w} : \mathbf{w}_l \in \mathcal{C}_{l,d} \forall l \in [L]\}$ completes the proof. \square

Remark. Note that in the special case of a full-width convolution the implicit regularizer reduces to $\mathcal{R}_{\mathcal{P}_{BWC}}(\beta) = \min_{\mathbf{w} : \mathcal{P}_{FWC}(\mathbf{w}) = \beta} \|\mathbf{w}\|_2^2 = \|\hat{\beta}\|_{2/L}$, as expected from [1]. In the general case, since each convolutional filter \mathbf{w}_l is constrained to be bounded-width (spatially limited), we can apply the Fourier Uncertainty Principle to prove that its frequency spectrum *cannot* be bounded-width (band limited) i.e., $\Delta(\hat{\mathbf{w}}_l) \geq 1/\Delta(\mathbf{w}_l) = O(1/d)$ where $\Delta(\cdot)$ is a reasonable measure of spread (e.g., standard deviation).

Next, to further investigate the origin of the high frequency bias, we asked: Is the effect of the bounded-width convolutional model also present in a model with only local kernels but not translation invariance? For this we trained a locally connected model with same kernel size on CIFAR10. In Figure 2 we observe that the locally connected models (LC and DLC) do not have as much energy in the higher frequencies, particularly for the deep models. This shows that local connectivity alone is *not* sufficient to learn high frequency features; translation invariance is also required. *Thus, local convolutions are necessary to obtain bias towards high frequency features, and therefore adversarial perturbations.* Importantly, we found the same results for CIFAR100, which has image statistics similar to CIFAR10. However, we did not for MNIST, which has no useful high frequency information (See Supp. Figure 9). This shows that an interaction between the implicit bias (induced by the model parametrization) and the dataset statistics is essential for high frequency features to be learned.

3.1.3 Testing IFR Hypothesis for Nonlinear models via the Injection of Hidden Shortcut Features

Given that the theory in [1] doesn't extend to the implicit regularization for nonlinear convolutional models, and our results on the relationship of $\hat{\beta}$ and $\hat{\delta}$, we decided to directly test if the nonlinear

Table 2: Performance on CIFAR-10 on base vs frequency-based dataset , mean \pm std over 5 trials each.

	Baseline	$\epsilon = .25, \rho = .2$	$\epsilon = .25, \rho = .1$
Fully Connected Linear	40.8 \pm .070	53.26 \pm .075	45.27 \pm 1.14
Fully Connected Nonlinear	48.5 \pm .084	59.6 \pm .223	54.93 \pm .497
Full Width Convolutional Linear	41.8 \pm .124	70.3 \pm .805	79.6 \pm 1.35
Full Width Convolutional Nonlinear	52.4 \pm 2.89	79.5 \pm .912	87.2 \pm 1.26
Bounded Width Convolutional Linear	41.8 \pm .046	97.28 \pm .604	92.33 \pm .679
Bounded Width Convolutional Nonlinear	56.7 \pm .489	98.8 \pm .850	97.8 \pm .475

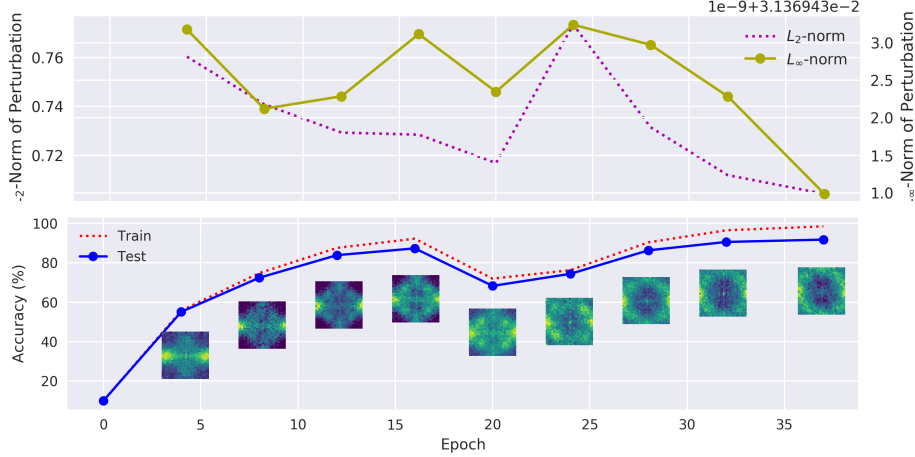


Figure 4: Top: Dynamics of ℓ_2 and ℓ_∞ norms of the adversarial perturbations (δ) during training of ResNet18. Over training, adversarial perturbations become smaller in amplitude (the norm increase after around 20 epochs is due to learning rate reset which decreases performance). Bottom: Evolution of the adversarial perturbation spectrum ($\hat{\delta}$) over training. The adversarial perturbation spectrum evolves from low-frequencies to high frequencies as performance increases.

bounded-width convolutional model is able to capture sparse frequency-based information in the dataset, thus confirming that the theory in [1] also holds for nonlinear models.

To test our hypothesis, we take inspiration from the field of steganography which focuses on hiding shortcut features in images that are visually undetectable by humans [32]. We introduced a class-correlated shortcut feature into every CIFAR-10 train and test set image. For each class, we sampled a $3 \times 32 \times 32$ matrix of scalars from a standard Gaussian, scaled by a factor $\epsilon = 0.25$ and with sparsity $\rho \in 0.1, 0.2$. Then, this class-specific shortcut feature was added into the Fourier spectrum of CIFAR-10 train and test images corresponding to their respective classes (See Figure 3):

$$\hat{\tilde{x}} = \hat{x} + \eta_{\text{class}} : M_{\text{class}} \odot (\epsilon * N_{\text{class}}), N_{\text{class}} \sim \mathcal{N}(0, 1), M_{\text{class}} \sim \text{Bernoulli}(\rho)$$

Our hypothesis is that these class-dependent sparse shortcut features will be mostly useful for model parameterizations that have an implicit regularizer that is sparse in the frequency domain. Therefore the model with the right implicit bias should achieve *higher* test accuracy.

Table 2 shows the test accuracy of each linear and nonlinear model with the new dataset and different levels of sparsity. We can observe that both the full-width and bounded-width models have higher performance than baseline with this new dataset. However, the fully connected model, having a different bias, cannot take full advantage of the class-dependent shortcut feature introduced into the dataset. This experiment reveals that the implicit regularizer for sparsity in the frequency domain is present in both linear and nonlinear convolutional models.

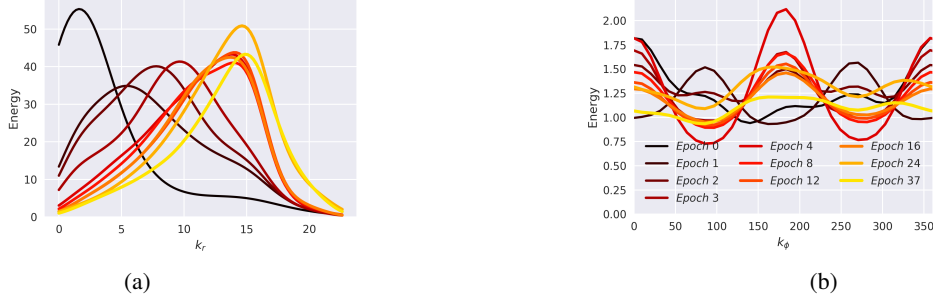


Figure 5: (a) Distribution of radial energy k_r of the Fourier spectrum of adversarial perturbations. (b) Distribution of angular energy k_ϕ (in degree) of the Fourier spectrum of adversarial perturbations. We observe an evolution of adversarial perturbations over training from lower to higher frequencies for the ResNet18 model, and from certain directions to all directions uniformly.

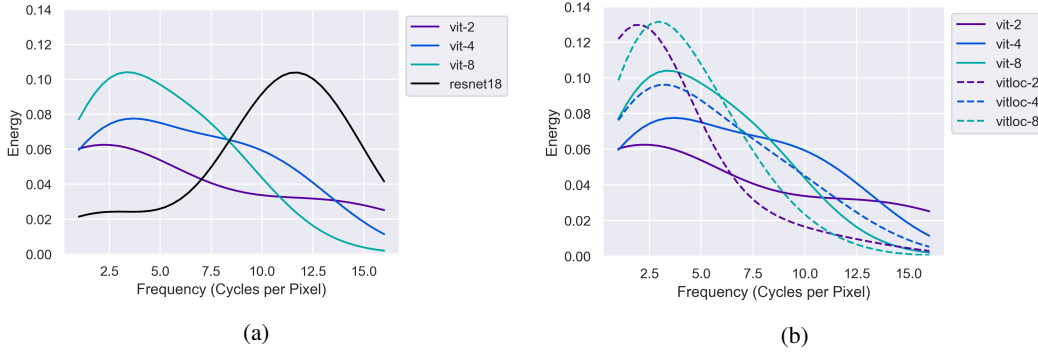


Figure 6: Radial Energy of the Adversarial Perturbations of Visual Transformer and Local Visual Transformer models. (a) All Visual Transformer models (vit-2, vit-4, vit-8) have more energy in lower frequencies than ResNet18. (b) Locally Connected model's (vitloc-2, vitloc-4, vitloc-8) spectrum have more energy in lower frequencies compared to their standard ViT counterpart.

3.2 Dynamics of Adversarial Examples in Frequency Domain

Here we hypothesize that during training the tension between the frequency dispersion and the sparsity promotion of convolutions is the cause of high frequency adversarial perturbations on state-of-the-art convolutional neural networks.

In order to test this hypothesis, we trained a ResNet18 model on the CIFAR-10 dataset [26] (MIT) using PyTorch [27]. Then, we used the Foolbox package [28] (MIT) to generate adversarial attacks for every example in the test set for intermediate models during training, via an ℓ_∞ Projected Gradient Descent attack [29] (see Sec. B.5). In Figure 4, we see the evolution of the frequency spectrum of the adversarial perturbations: early in training the adversarial perturbations tend to contain low frequencies (with higher norms), and as training progresses, there is a consistent evolution towards higher frequencies (with lower norms). Thus, adversarial perturbations evolve through learning to higher frequencies and lower amplitudes.

This phenomenon is also confirmed in Figures 5a and 5b. Here, we observe the marginal radial and angular distributions $E(k_r)$, $E(k_\phi)$ of the energy spectrum $E(k_r, k_\phi) := |\hat{\delta}(k_r \cos k_\phi, k_r \sin k_\phi)|_{\mathbb{C}}^2$, where (k_r, k_ϕ) denotes polar coordinates in the frequency domain. We also observe that (i) the radial energy distribution shifts from low to high frequency, and (ii) the angular energy distribution becomes more uniform (ring structure). The evolution of the adversarial perturbations in the frequency domain shows an optimization bias of state-of-the-art convolutional models to frequency-based features.

3.3 Visual Transformers do not exhibit a high frequency bias

Since local convolutions cause a bias towards high frequency features and adversarial perturbations, it is natural to ask: Are high-performance deep models without convolutions less biased towards high-frequency features? One possible architecture is the Visual Transformer (ViT), which has performed on par with convolution-based architectures in many tasks including object recognition [18]. Furthermore, recent work has shown that ViTs can be more robust to high frequency adversarial perturbations than ResNets [33].

We hypothesize that the lack of convolutional operations in ViTs is responsible for this greater robustness to high frequency attacks. In order to test this, we trained a ViT with different patch sizes on CIFAR-10 (See Supp. Sec. B.4 for training details). All of these models achieved about 80% test accuracy. Then, we attacked these models with a PGD-Linf attack, the same used earlier in the paper. In Figure 6a, we observe the average frequency spectrum of ViTs with different word/patch sizes (2×2 , 4×4 , 8×8), as compared to a ResNet18 with similar test accuracy (we stopped the training when the model had near 80% test accuracy). We observe that all of the ViTs have more energy in the lower frequencies than the ResNet18. This strongly suggests that the robustness to high frequency attacks shown in [33] might be due to the lack of convolution layers. Furthermore, we observe that different patch/word sizes also have an impact on the spectrum, with smaller word sizes producing higher frequency spectra. This is consistent with the theoretical and empirical results comparing full-width and bounded-width convolutional models in Section 3.1.1.

However, as others have suggested [34], some layers of the ViT can still be interpreted as convolutional layers, so the model is not entirely convolution-free. In particular, the first embedding layer is shared across all image patches, and therefore can be interpreted as a convolutional layer with stride equal to the patch/kernel size. This leads us to ask: Can we remove this layer and shift the energy spectrum to even lower frequencies? To test this we defined a new ViT architecture in which we removed the weight sharing in the first layer patch embedding by using a locally connected layer with the same kernel size and stride as the convolutional version, so that each patch has independent weights. We call this architecture the Visual Local Transformer (ViTLoc). Then, we trained this architecture on CIFAR-10 (see Performance in Sup. Table 6) and computed its adversarial perturbations. In Figure 6b, we observe that every ViTLoc model has a lower frequency spectrum than its ViT counterpart. This is more evidence that avoiding the convolutional parametrization, even in very complex state-of-the-art models, can reduce the high frequency bias, and therefore, high frequency adversarial perturbations.

4 Conclusions and Future Work

We provide both empirical as well as theoretical evidence that the high-frequency nature of adversarial examples is due to the bounded-width convolutional architecture of modern high-performance CNNs. To this end, we first showed that theoretical results in deep linear full-width convolutional models [1] extend to nonlinear models. Second, we derived new theoretical results for the implicit bias of deep linear bounded-width convolutions, showing that such networks are biased towards high-frequency features. Further, using a novel steganography experiment, we could clearly confirm that this bias extends to nonlinear models (including ResNet-18), and that it strongly influences the features learned by the models.

In line with these results, we find that the Visual Transformer architecture, which features almost no explicit convolutions, is less biased towards high frequencies. We demonstrated that by removing one of the only convolutional layers in the model (ViTLoc Architecture), this bias can be reduced even further. We think this is important because ViT, similar to ResNets, have multiple components such as Norm Layers, Skip Connections, Attention, etc, that should affect the implicit bias of the model. However, we found that the linear layer parametrization seem to be crucial to the nature of the features learned and therefore for the adversarial perturbations.

We think this work will be important for assessing bias and fairness in bias in machine learning. Much work has been centered around bias in datasets, however, here we show that attention needs to be paid to bias caused by architectural choices as well. For example, How does this type of bias affect networks for facial recognition, surveillance, self-driving cars, etc? We hope this work will help us take a step toward auditing of model decisions and encouraging more human-interpretable features.

Our results are clearly just the beginning of understanding how implicit bias shapes adversarial perturbations, and much is left to be understood. However, we believe that a better understanding of the implicit bias can help drive models towards the most useful set of features and reduce the adversarial susceptibility of modern neural networks.

Acknowledgments

This research has been funded by the NSF NeuroNex program through grant DBI-1707400. This research was also supported by Intelligence Advanced Research Projects Activity (IARPA) via Department of Interior/Interior Business Center (DoI/IBC) contract number D16PC00003. The U.S. Government is authorized to reproduce and distribute reprints for Governmental purposes notwithstanding any copyright annotation thereon. Disclaimer: The views and conclusions contained herein are those of the authors and should not be interpreted as necessarily representing the official policies or endorsements, either expressed or implied, of IARPA, DoI/IBC, or the U.S. Government.

References

- [1] Suriya Gunasekar, Jason D Lee, Daniel Soudry, and Nati Srebro. Implicit bias of gradient descent on linear convolutional networks. In *Advances in Neural Information Processing Systems*, pages 9461–9471, 2018.
- [2] Justin Gilmer, Luke Metz, Fartash Faghri, Samuel S Schoenholz, Maithra Raghu, Martin Wattenberg, and Ian Goodfellow. Adversarial spheres. *arXiv preprint arXiv:1801.02774*, 2018.
- [3] Saeed Mahloujifar, Dimitrios I Diochnos, and Mohammad Mahmood. The curse of concentration in robust learning: Evasion and poisoning attacks from concentration of measure. In *Proceedings of the AAAI Conference on Artificial Intelligence*, volume 33, pages 4536–4543, 2019.
- [4] Thomas Tanay and Lewis Griffin. A boundary tilting perspective on the phenomenon of adversarial examples. *arXiv preprint arXiv:1608.07690*, 2016.
- [5] Nic Ford, Justin Gilmer, Nicolas Carlini, and Dogus Cubuk. Adversarial examples are a natural consequence of test error in noise. *arXiv preprint arXiv:1901.10513*, 2019.
- [6] Alhussein Fawzi, Hamza Fawzi, and Omar Fawzi. Adversarial vulnerability for any classifier. In *Advances in Neural Information Processing Systems*, pages 1178–1187, 2018.
- [7] Sébastien Bubeck, Eric Price, and Ilya Razenshteyn. Adversarial examples from computational constraints. *arXiv preprint arXiv:1805.10204*, 2018.
- [8] Ian J Goodfellow, Jonathon Shlens, and Christian Szegedy. Explaining and harnessing adversarial examples. *arXiv preprint arXiv:1412.6572*, 2014.
- [9] Ludwig Schmidt, Shibani Santurkar, Dimitris Tsipras, Kunal Talwar, and Aleksander Madry. Adversarially robust generalization requires more data. In *Advances in Neural Information Processing Systems*, pages 5014–5026, 2018.
- [10] Dong Yin, Raphael Gontijo Lopes, Jon Shlens, Ekin Dogus Cubuk, and Justin Gilmer. A fourier perspective on model robustness in computer vision. In *Advances in Neural Information Processing Systems*, pages 13255–13265, 2019.
- [11] Chulhee Yun, Shankar Krishnan, and Hossein Mobahi. A unifying view on implicit bias in training linear neural networks. *arXiv preprint arXiv:2010.02501*, 2020.
- [12] Justin Sahs, Aneel Damaraju, Ryan Pyle, Onur Tavaslioglu, Josue Ortega Caro, Hao Yang Lu, and Ankit Patel. A functional characterization of randomly initialized gradient descent in deep re{lu} networks, 2020. URL <https://openreview.net/forum?id=BJ19PRVKDS>.
- [13] Francis Williams, Matthew Trager, Daniele Panozzo, Claudio Silva, Denis Zorin, and Joan Bruna. Gradient dynamics of shallow univariate relu networks. In *Advances in Neural Information Processing Systems*, pages 8376–8385, 2019.

- [14] Blake Woodworth, Suriya Gunasekar, Jason D Lee, Edward Moroshko, Pedro Savarese, Itay Golan, Daniel Soudry, and Nathan Srebro. Kernel and rich regimes in overparametrized models. *arXiv preprint arXiv:2002.09277*, 2020.
- [15] Justin Sahs, Ryan Pyle, Aneel Damaraju, Josue Ortega Caro, Onur Tavaslioglu, Andy Lu, and Ankit Patel. Shallow univariate relu networks as splines: Initialization, loss surface, hessian, & gradient flow dynamics. *arXiv preprint arXiv:2008.01772*, 2020.
- [16] Zhiyuan Li, Ruosong Wang, Dingli Yu, Simon S Du, Wei Hu, Ruslan Salakhutdinov, and Sanjeev Arora. Enhanced convolutional neural tangent kernels. *arXiv preprint arXiv:1911.00809*, 2019.
- [17] Sanjeev Arora, Simon S Du, Wei Hu, Zhiyuan Li, Russ R Salakhutdinov, and Ruosong Wang. On exact computation with an infinitely wide neural net. In *Advances in Neural Information Processing Systems*, pages 8139–8148, 2019.
- [18] Alexey Dosovitskiy, Lucas Beyer, Alexander Kolesnikov, Dirk Weissenborn, Xiaohua Zhai, Thomas Unterthiner, Mostafa Dehghani, Matthias Minderer, Georg Heigold, Sylvain Gelly, et al. An image is worth 16x16 words: Transformers for image recognition at scale. *arXiv preprint arXiv:2010.11929*, 2020.
- [19] Andrew Ilyas, Shibani Santurkar, Dimitris Tsipras, Logan Engstrom, Brandon Tran, and Aleksander Madry. Adversarial examples are not bugs, they are features. In *Advances in Neural Information Processing Systems*, pages 125–136, 2019.
- [20] Evgenia Rusak, Lukas Schott, Roland Zimmermann, Julian Bitterwolf, Oliver Bringmann, Matthias Bethge, and Wieland Brendel. Increasing the robustness of dnns against image corruptions by playing the game of noise. *arXiv preprint arXiv:2001.06057*, 2020.
- [21] Ali Shafahi, W Ronny Huang, Christoph Studer, Soheil Feizi, and Tom Goldstein. Are adversarial examples inevitable? *arXiv preprint arXiv:1809.02104*, 2018.
- [22] Cihang Xie, Mingxing Tan, Boqing Gong, Jiang Wang, Alan Yuille, and Quoc V Le. Adversarial examples improve image recognition. *arXiv preprint arXiv:1911.09665*, 2019.
- [23] Dimitris Tsipras, Shibani Santurkar, Logan Engstrom, Alexander Turner, and Aleksander Madry. Robustness may be at odds with accuracy. *arXiv preprint arXiv:1805.12152*, 2018.
- [24] Preetum Nakkiran. Adversarial robustness may be at odds with simplicity. *arXiv preprint arXiv:1901.00532*, 2019.
- [25] Gauthier Gidel, Francis Bach, and Simon Lacoste-Julien. Implicit regularization of discrete gradient dynamics in linear neural networks. In *Advances in Neural Information Processing Systems*, pages 3196–3206, 2019.
- [26] Alex Krizhevsky, Geoffrey Hinton, et al. Learning multiple layers of features from tiny images. 2009.
- [27] Adam Paszke, Sam Gross, Soumith Chintala, Gregory Chanan, Edward Yang, Zachary DeVito, Zeming Lin, Alban Desmaison, Luca Antiga, and Adam Lerer. Automatic differentiation in pytorch. 2017.
- [28] Jonas Rauber, Wieland Brendel, and Matthias Bethge. Foolbox: A python toolbox to benchmark the robustness of machine learning models. *arXiv preprint arXiv:1707.04131*, 2017.
- [29] Alexey Kurakin, Ian Goodfellow, and Samy Bengio. Adversarial examples in the physical world. *arXiv preprint arXiv:1607.02533*, 2016.
- [30] Wieland Brendel, Jonas Rauber, Matthias Kümmerer, Ivan Ustyuzhaninov, and Matthias Bethge. Accurate, reliable and fast robustness evaluation. In *Advances in Neural Information Processing Systems*, pages 12861–12871, 2019.
- [31] Gabriel Goh. A discussion of 'adversarial examples are not bugs, they are features': Two examples of useful, non-robust features. *Distill*, 2019. doi: 10.23915/distill.00019.3. <https://distill.pub/2019/advex-bugs-discussion/response-3>.

- [32] Abbas Cheddad, Joan Condell, Kevin Curran, and Paul Mc Kevitt. Digital image steganography: Survey and analysis of current methods. *Signal processing*, 90(3):727–752, 2010.
- [33] Rulin Shao, Zhouxing Shi, Jinfeng Yi, Pin-Yu Chen, and Cho-Jui Hsieh. On the adversarial robustness of visual transformers. *arXiv preprint arXiv:2103.15670*, 2021.
- [34] Zhengsu Chen, Lingxi Xie, Jianwei Niu, Xuefeng Liu, Longhui Wei, and Qi Tian. Visformer: The vision-friendly transformer. *arXiv preprint arXiv:2104.12533*, 2021.

A Additional Figures & Tables

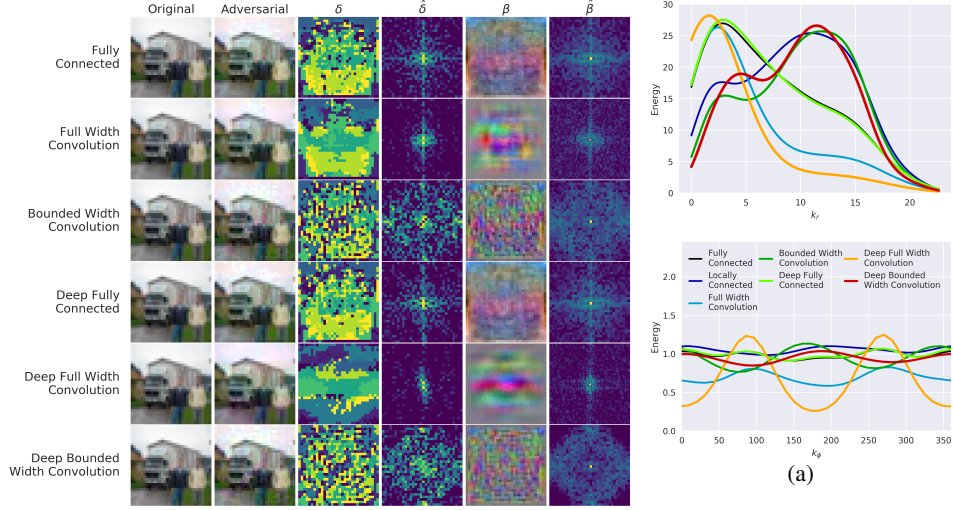


Figure 7: (a) Example Visualization of δ , $\hat{\delta}$, β and $\hat{\beta}$ for 6 overparametrized linear models with one hidden layer. We observe qualitatively (particularly in $\hat{\beta}$) that both full width and bounded width convolutional models are sparser than the Fully Connected model. For quantification, see Table 3. (b) Radial (top, k_r) and Angular (bottom, k_ϕ in degree) of $\hat{\delta}$.

Table 3: Frequency-Domain Norms of Predictor $\hat{\beta}$ and Adv. Pert. $\hat{\delta}$ for Linear Models. With Equivalent performance (See Sup Figure 6), Convolutional Models have smaller $\|\hat{\beta}\|_1$, supporting the implicit Fourier hypothesis.

Model	$\ \hat{\delta}\ _2$	$\ \hat{\delta}\ _1$	$\ \hat{\beta}\ _2$	$\ \hat{\beta}\ _1$
Fully Connected	20.77 ± 1.23	505.95 ± 32.22	546.89 ± 43.37	2232.46 ± 166.27
Full Width Convolution	17.52 ± 1.56	376.31 ± 32.66	544.83 ± 42.40	1598.37 ± 181.44
Bounded Width Convolution	20.65 ± 1.09	556.32 ± 32.64	500.67 ± 47.46	2623.04 ± 331.42
Deep Fully Connected	20.83 ± 1.25	503.92 ± 32.62	554.16 ± 38.95	2168.06 ± 134.07
Deep Full Width Convolution	17.13 ± 1.68	265.40 ± 41.72	522.99 ± 39.72	1417.68 ± 213.91
Deep Bounded Width Convolution	20.57 ± 0.94	550.30 ± 29.71	498.52 ± 47.15	2392.09 ± 278.55

Table 4: Frequency-Domain Norms of Adv. Pert. $\hat{\delta}$ for Nonlinear Models. With similar performance (Supp. Table 3), Full Width and Bounded Width convolutional models produce adversarial attacks with smaller $\|\hat{\delta}\|_1$.

Model	$\ \hat{\delta}\ _2$	$\ \hat{\delta}\ _1$
Fully Connected	22.06 ± 1.35	534.34 ± 35.93
Locally Connected	22.32 ± 1.13	587.61 ± 29.89
Full Width Convolution	20.57 ± 1.11	405.49 ± 34.16
Bounded Width Convolution	24.63 ± 1.36	665.22 ± 38.55
Shallow ResNet	26.36 ± 0.74	709.06 ± 20.76
VGG19	23.32 ± 0.99	650.73 ± 27.87
ResNet18	22.42 ± 0.91	626.60 ± 25.40

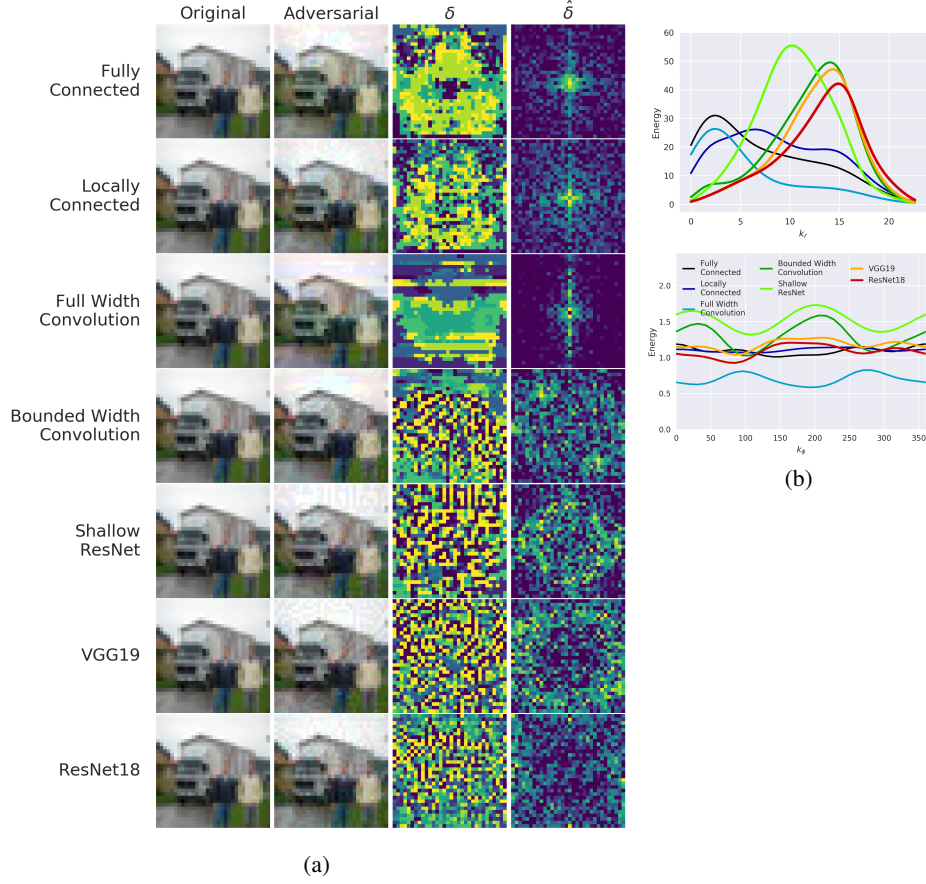


Figure 8: (a) Visualization of the average of the spectra $\hat{\delta}_n$ over all sampled inputs n for all nonlinear models. The average spectra are similar to the examples observed in Figure 8. (b) Radial (top, k_r) and Angular (bottom, k_ϕ in degree) of $\hat{\delta}$. Distribution of Energy in $\hat{\delta}$ show that deep, bounded-Width models shift energy into higher frequencies, and the angular energy of Fully Connected and Locally Connected models are distributed more uniformly.

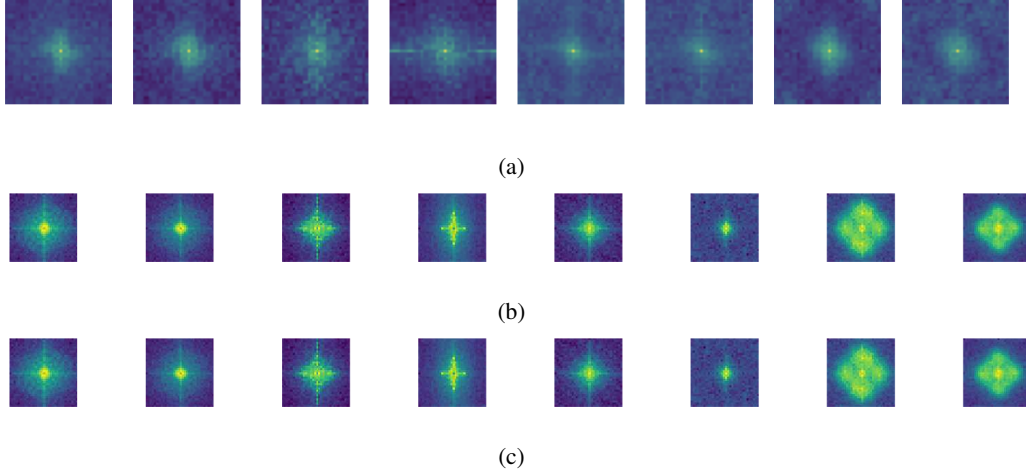


Figure 9: Adversarial Spectrum for: Fully Connected, Deep Fully Connected, Full-Width Convolutional, Deep Full-Width Convolutional, Locally Connected, Deep Fully Connected, Bounded-Width Convolutional, Deep Bounded Width Convolutional models for a) MNIST (Linear Models), b) CIFAR100 (Linear Models) and c) CIFAR100 (NonLinear Models). Both CIFAR100 results are similar to the CIFAR10 experiments. No difference between MNIST models

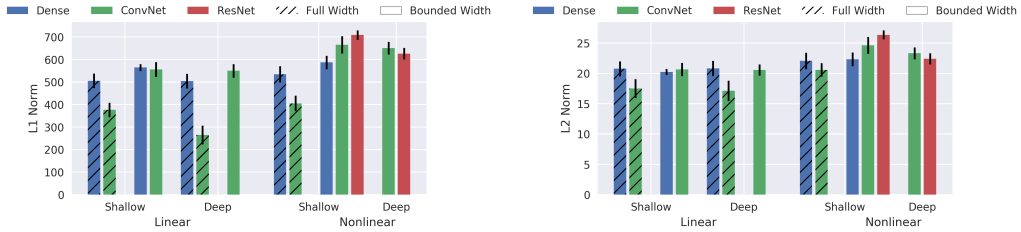


Figure 10: Comparison of Adversarial Perturbation Norms $\|\hat{\delta}\|_p$ for $p = 1, 2$ for different linear and nonlinear models. The relations between norms of nonlinear models mirror and accentuate those of linear models. See Sections 3.2 for detailed comparisons.

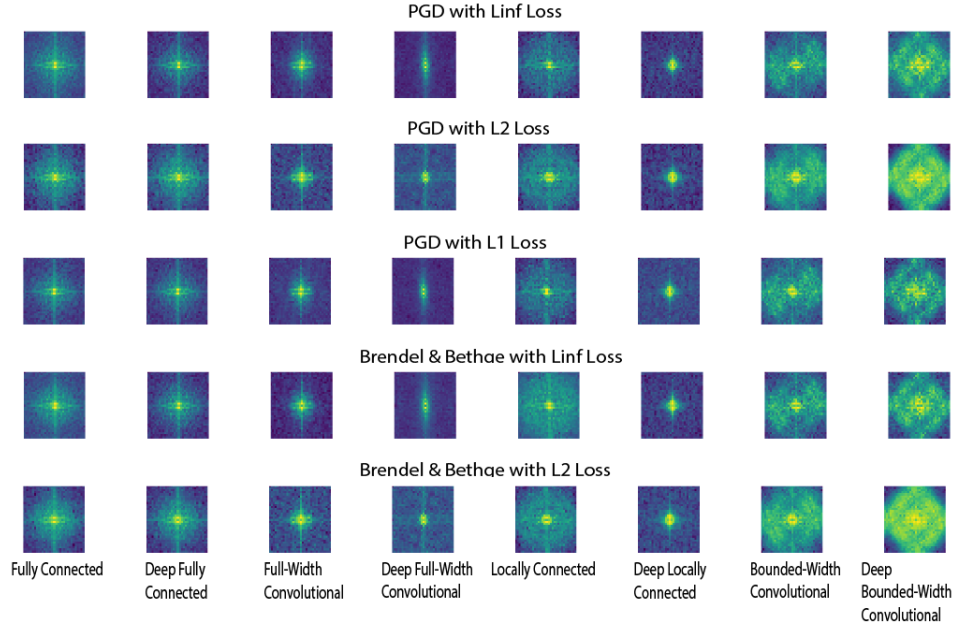


Figure 11: Average Adversarial Perturbation Fourier Spectrum for Fully Connected, Full-Width, Locally Connected and Bounded-Width **Linear** models.

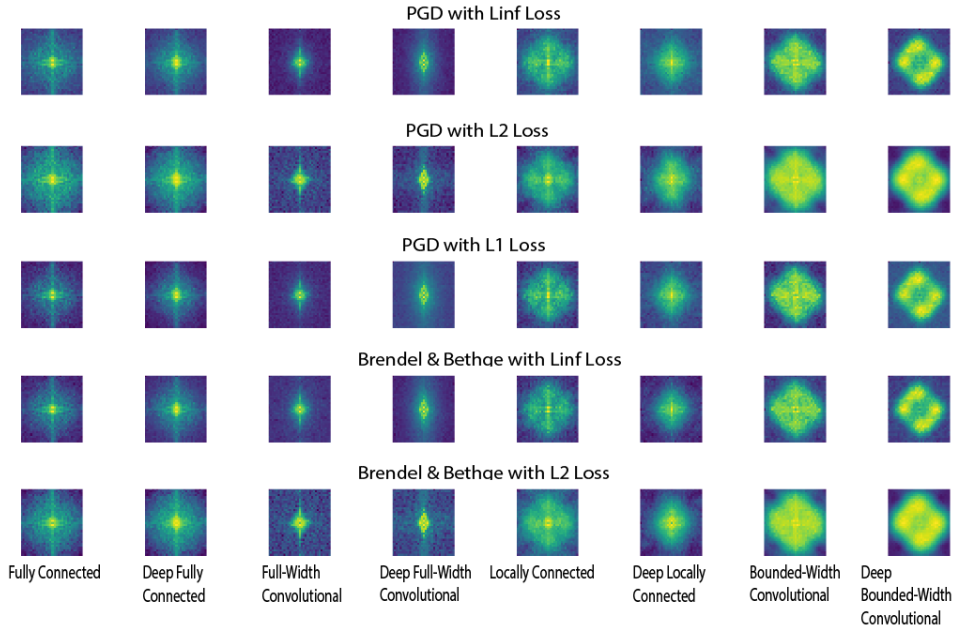


Figure 12: Average Adversarial Perturbation Fourier Spectrum for Fully Connected, Full-Width, Locally Connected and Bounded-Width **NonLinear** models.

B Experimental Details

B.1 Model Architectures

Table 5: Model Architectures

Model Architecture	# Hidden Layers	Nonlinearity	Channels
Fully Connected	1,3	None, ReLU	2700
Bounded Width Convolution	1,3	None, ReLU	(3,32)
Full Width Convolution	1,3	None, ReLU	3
Locally Connected	1	None, ReLU	32

B.2 Model Performance

Table 6: Test Accuracy for all models trained on CIFAR-10. All linear models have similar performance. Nonlinear models exhibit more variability.

Model Architecture	Test Accuracy
Fully Connected (Linear)	41%
Locally Connected (Linear)	35%
Full Width Convolution (Linear)	41%
Bounded Width Convolution (Linear)	41%
Deep Fully Connected (Linear)	41%
Deep Full Width Convolution (Linear)	36%
Deep Bounded Width Convolution (Linear)	41%
Fully Connected (NonLinear)	52%
Full-Width Convolution (NonLinear)	52%
Locally Connected (NonLinear)	54%
Bounded Width Convolution (NonLinear)	63%
ViT-2	79.8%
ViT-4	80.1%
ViT-8	78.4%
ViTLoc-2	75.3%
ViTLoc-4	80.2%
ViTLoc-8	74.5%
ResNet18	92%

All models were trained on a single GTX 1080 Ti for 30 to 120 GPU minutes.

B.3 Adversarial Attack Success

Table 7: Adversarial Success for all models trained on CIFAR-10. All values are shown for PGD-Linf of B.5

Model Architecture	Adversarial Success (PGD-Linf)
Fully Connected (Linear)	100.0%
Locally Connected (Linear)	100.0%
Full Width Convolution (Linear)	100.0%
Bounded Width Convolution (Linear)	100.0%
Deep Fully Connected (Linear)	100.0%
Deep Full Width Convolution (Linear)	100.0%
Deep Bounded Width Convolution (Linear)	100.0%
Fully Connected (NonLinear)	100.0%
Full-Width Convolution (NonLinear)	100.0%
Locally Connected (NonLinear)	100.0%
Bounded Width Convolution (NonLinear)	100.0%
ViT-2	100.0%
ViT-4	99.7%
ViT-8	100.0%
ViTLoc-2	100.0%
ViTLoc-4	100.0%
ViTLoc-8	99.9%
ResNet18	100.0%

All adversarial attacks were performed on a single GTX 1080 Ti for all 10 thousand testset images.

B.4 Training Hyperparameters

Table 8: Learning rates for the various models considered on CIFAR-10. All other hyper-parameters were fixed.

Model Architecture	Learning Rate	Batch Size	Learning Rate Drop
Bounded Width Convolution	.01	128	Yes
Fully Connected	.01	128	Yes
Locally Connected	.01	128	Yes
Full Width Convolution	.002	128	Yes
Bounded Width Convolution	.002	128	Yes

Table 9: Learning rates for the various models considered on CIFAR-100. All other hyper-parameters were fixed.

Model Architecture	Learning Rate	Batch Size	Learning Rate Drop
Bounded Width Convolution	.01	128	Yes
Fully Connected	.01	128	Yes
Locally Connected	.01	128	Yes
Full Width Convolution	.002	128	Yes
Bounded Width Convolution	.002	128	Yes

Table 10: Learning rates for the various models considered on MNIST. All other hyper-parameters were fixed.

Model Architecture	Learning Rate	Batch Size	Learning Rate Drop
Bounded Width Convolution	.01	100	Yes
Fully Connected	.01	100	Yes
Locally Connected	.01	100	Yes
Full Width Convolution	.002	100	Yes
Bounded Width Convolution	.002	100	Yes

Learning Rates. We tuned the max learning rates for each model by starting from a base learning rate of 0.1, and then, if there were visible failures during training (most commonly, the model converging to chance performance), we adjusted the learning rate up/down by a factor of 10 or 50.

Amongst the model architectures we explored, the only hyper-parameter that was tuned was the learning rate. The final values of the learning rates after search are detailed in Table 8.

In addition, all the models were trained with linearly decaying learning rate follow 0.3 factor for each epoch and resetting the learning rate back to max when you trained the model at least 20 epochs. All models were trained for at least 40 epochs and we choose the epoch with the highest accuracy for further experiments.

B.5 Adversarial Attack Configurations

Table 11: Adversarial Attack hyperparameters

Attack	Metric	Learning Rate	Number of Steps	Max Norm, ϵ
Projected Gradient Descent	L_∞	0.1	1000	8.0/255.0
Projected Gradient Descent	L_2	0.1	1000	2.0
Projected Gradient Descent	L_1	0.1	200	0.1
Brendel-Bethge Attack	L_∞	1e-03	1000	-
Brendel-Bethge Attack	L_2	1e-03	1000	-

Learning Rates. All the models adversarial attacks were generated using the configuration above with the Foolbox package [28].